Oscillatory shear rheology measurements and Newtonian modeling of insoluble monolayers

Fayaz Rasheed, Aditya Raghunandan, Amir H. Hirsa, and Juan M. Lopez

Phys. Rev. Fluids **2**, 044002 — Published 5 April 2017

DOI: 10.1103/PhysRevFluids.2.044002

Oscillatory shear rheology measurements and Newtonian modeling of insoluble monolayers

Fayaz Rasheed, Aditya Raghunandan, and Amir H. Hirsa

Department of Mechanical, Aerospace and Nuclear Engineering,

Rensselaer Polytechnic Institute, Troy, NY 12180-3590, USA

Juan M. Lopez*

School of Mathematical and Statistical Sciences,

Arizona State University, Tempe, Arizona 85287, USA

(Dated: March 8, 2017)

Abstract

Circular systems are advantageous for interfacial studies since they do not suffer from end effects, but their hydrodynamics is more complicated because their flows are not uni-directional. Here, we analyze the shear rheology of a harmonically-driven knife-edge viscometer through experiments and computations based on the Navier-Stokes equations with a Newtonian interface. The measured distribution of phase lag in the surface velocity relative to the knife-edge speed is found to have a good signal-to-noise ratio and provides robust comparisons to the computations. For monomolecular films of stearic acid, the surface shear viscosity deduced from the model was found to be the same whether the film is driven steady or oscillatory, for an order of magnitude range in driving frequencies and amplitudes. Results show that increasing either the amplitude or forcing frequency steepens the phase lag next to the knife edge. In all cases, the phase lag is linearly proportional to the radial distance from the knife edge and scales with surface shear viscosity to the power $-1/2$.

* jmlopez@asu.edu

I. INTRODUCTION

Monomolecular films on liquids can drastically alter the transfer of mass, momentum, and energy across the surface of the liquid due to the coupling to the bulk hydrodynamics. The importance of monolayers on hydrodynamics is evident everywhere we look in nature, ranging from small scale systems such as the alveoli in the lungs [1–4] to CO_2 exchange between the atmosphere and the oceans [5–8]. In manufacturing, monolayers on liquids impact everything from micro-electronics to the production of polyurethane foam [9, 10]. Other man-made systems dominated by interfacial phenomena include ink-jet printers [11, 12] and emulsifiers in food processing [13, 14]. A recent development in the pharmaceutical industry is an increasing reliance on interfacial processing [15]. Yet, it is surprising how limited our knowledge is of interfacial hydrodynamics and its prediction.

When sheared, many monolayers on liquids exhibit an intrinsic or "excess" surface viscosity. In both biological and man-made systems, we often wish to understand the response of interfaces to oscillatory forcing, which is complicated because although the interface has no inertia, the liquid with which it is in contact does have mass and a finite amount of inertia. Therefore, even for systems with very high surface shear viscosity, the effect of the bulk liquid cannot be ignored when considering unsteady processes.

Recently, Verwijlen *et al.* [16] provided a theoretical foundation for the analysis of the harmonically-driven magnetic needle surface viscometer. Their theory included the coupling of the interfacial and bulk flows. One of the fundamental challenges with the utilization of the magnetic needle is the problem of end effects: the finite needle is three-dimensional but the theory is planar.

Circular systems have long been popular for interfacial flow studies since they do not suffer from end effects. Although the use of a circular needle or a knife edge (similar to the needle, but does not penetrate the liquid substrate) eliminates end-effect issues, it complicates the analysis because the flow is not uni-directional. That is because unlike in the planar case, where the vorticity vector only has one component and is orthogonal to the uni-directional flow, in curved systems vortex line bending produces a secondary flow, resulting in both the vorticity and the velocity vectors having three non-zero components. Even at low speeds, when inertia is not important, vortex line bending still exists and drives a secondary flow. It was shown in [17] that the secondary flow scales with the Reynolds number, and can only be

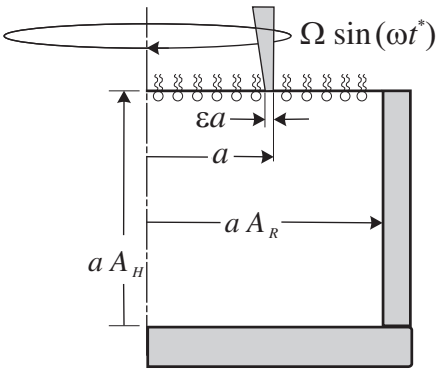

FIG. 1. Schematic of the oscillatory knife-edge viscometer, denoting the dimensional quantities. The origin of the coordinate system is on the axis at the bottom endwall.

ignored when $Re \to 0$. However, experiments typically have $Re \sim 10^2 - 10^3$, and so analyses which assume uni-directional flow are not valid, even with the coupling between bulk and interfacial flows being taken into account, because the flow in the bulk is not uni-directional [18].

Here, we present a numerical model to fully account for the effect of bulk flow on oscillatory sheared interfaces. The predictions are compared directly to time-resolved measurements of the interfacial velocity. The measurements and computations show a phase lag in the interfacial velocity relative to the instantaneous velocity of the knife edge which increases linearly with the radial distance from the knife edge. The phase lag results from the coupling between the interfacial and bulk flows. The radial gradient of the phase lag is found to depend strongly on the surface shear viscosity. A steady streaming meridional bulk flow is found to result from the oscillatory azimuthal motion of the interface. The response of the monolayer to steady shear was also measured and gave a consistent value of surface shear viscosity regardless of whether the film was subjected to steady or oscillatory shear.

II. GOVERNING EQUATIONS

Consider a stationary cylinder of radius aA_R, filled to a depth aA_H with water of dynamic viscosity μ and kinematic viscosity ν. The top surface is uniformly covered by a monolayer and the flow is driven by the oscillatory rotation of a knife edge of outer radius a and thickness ϵa that just touches the monolayer. The knife edge has a maximum angular speed

of Ω and the frequency of oscillation is ω. Figure 1 shows a schematic of this set-up.

The governing equations are the Navier–Stokes equations with no-slip boundary conditions on the cylinder wall and floor together with the tangential stress balance at the air-water interface, and no-slip at the oscillating knife. Using a as the length scale and $1/\Omega$ as the time scale, and assuming the flow to remain axisymmetric, the non-dimensional Navier–Stokes equations are written in cylindrical coordinates (r, θ, z), with the velocity in terms of the stream-function, ψ, and angular momentum, γ,

$$\boldsymbol{u} = (u, v, w) = (-1/r\,\partial\psi/\partial z,\ \gamma/r,\ 1/r\,\partial\psi/\partial r), \tag{1}$$

and the vorticity

$$\nabla \times \boldsymbol{u} = (-1/r\,\partial\gamma/\partial z,\ \eta,\ 1/r\,\partial\gamma/\partial r), \tag{2}$$

resulting in

$$\frac{\partial\gamma}{\partial t} - \frac{1}{r}\frac{\partial\psi}{\partial z}\frac{\partial\gamma}{\partial r} + \frac{1}{r}\frac{\partial\psi}{\partial r}\frac{\partial\gamma}{\partial z} = \frac{1}{Re}\left(\frac{\partial^2\gamma}{\partial z^2} + \frac{\partial^2\gamma}{\partial r^2} - \frac{1}{r}\frac{\partial\gamma}{\partial r}\right), \tag{3}$$

$$\frac{\partial\eta}{\partial t} - \frac{1}{r}\frac{\partial\psi}{\partial z}\frac{\partial\eta}{\partial r} + \frac{1}{r}\frac{\partial\psi}{\partial r}\frac{\partial\eta}{\partial z} + \frac{\eta}{r^2}\frac{\partial\psi}{\partial z} - \frac{2\gamma}{r^3}\frac{\partial\gamma}{\partial z} = \frac{1}{Re}\left(\frac{\partial^2\eta}{\partial z^2} + \frac{\partial^2\eta}{\partial r^2} + \frac{1}{r}\frac{\partial\eta}{\partial r} - \frac{\eta}{r^2}\right), \tag{4}$$

$$\frac{\partial^2\psi}{\partial z^2} + \frac{\partial^2\psi}{\partial r^2} - \frac{1}{r}\frac{\partial\psi}{\partial r} = -r\eta, \tag{5}$$

where $Re = \Omega a^2/\nu$ is the Reynolds number.

Geometric parameters describing this system are the ratio of cylinder radius to the outer knife-edge radius, A_R, and water depth to outer knife-edge radius ratio, A_H. Another geometric parameter is the ratio of the knife-edge thickness to its outer radius, ϵ. The experiments and the simulations keep these fixed at $A_R = A_H = 5.25$ and $\epsilon = 0.167$.

The no-slip boundary conditions on the stationary cylinder walls are:

$$\text{Sidewall, } r = A_R: \quad \gamma = \psi = 0, \eta = -\frac{1}{A_R}\frac{\partial^2\psi}{\partial r^2}, \tag{6}$$

$$\text{Bottom, } z = 0: \quad \gamma = \psi = 0, \eta = -\frac{1}{r}\frac{\partial^2\psi}{\partial z^2}. \tag{7}$$

The interfacial and bulk flows are coupled via stress balances. For a flat interface, the velocity normal to the interface vanishes. Insoluble monolayers on water that are of sufficient concentration to exhibit surface shear viscosity are generally stiff enough to resist radial motion, as only a very small surface tension gradient is required to overcome the radial

interfacial velocity component [19]. These considerations reduce the radial and normal stress balances at the interface to

$$\eta = -\frac{1}{r}\frac{\partial^2 \psi}{\partial z^2} \quad \text{and} \quad \psi = 0 \quad \text{at } z = A_H. \tag{8}$$

This leaves only the azimuthal stress balance. For a Newtonian interface whose only nonzero velocity is in the azimuthal direction, the azimuthal tangential stress balance is described using the Boussinesq–Scriven surface model [20–22], giving

$$\frac{\partial^2 v}{\partial r^2} + \frac{1}{r}\frac{\partial v}{\partial r} - \frac{v}{r^2} = \frac{1}{Bo}\frac{\partial v}{\partial z}, \quad \text{at } z = A_H, \tag{9}$$

where $Bo = \mu^s/\mu a$ is the Boussinesq number, μ^s is the surface shear viscosity, and μ is the dynamic viscosity of the bulk liquid.

The interface is not a singly-connected surface due to the contact with the knife edge; the interfacial conditions (8) and (9) are enforced on the interface $r \in [0, 1-\epsilon) \cup (1, A_R)$, and no-slip is imposed on the knife edge:

$$v(r, A_H) = \sin(St\, t), \ \psi = 0, \ \text{and } \eta = -\frac{1}{r}\frac{\partial^2 \psi}{\partial z^2} \quad \text{for } r \in [1-\epsilon, 1], \tag{10}$$

where $St = \omega/\Omega$ is the Stokes number.

A. Numerical technique

The Navier–Stokes equations, (3), (4) and (5), are solved in the bulk using a second-order centered finite-difference discretization in space and a second-order predictor-corrector (Heun's method) for time advancement. The method has been used and tested on internal rotating flows [23]. It has also been extended to handle viscous and inviscid monolayers [19, 24], and in particular for the steady knife-edge viscometer [17, 25]. The same implementation is used here, where (8), (9) and (10) are imposed at the interface. Knowing the interior bulk flow at any point in time, (8) is evaluated using second-order one-sided differences. As in other implementations [17, 19, 25], (9) is solved for v at the interface at each point in time with the just-computed interior solution v which is used to determine $\partial v/\partial z$ using second-order one-sided differences. The only essential modification from the code used in [17] is the time-periodic boundary condition at the knife edge, and this is straight-forward to implement. Grid resolution studies were conducted in [17]; for the present study, the

number of grid points used in the r and z directions was $n_r = n_z = 527$, giving 17 grid points for the knife edge. The time-step δt depends mainly on Re and St, and particular attention was given to ensure that a sufficient number of time steps per forcing period were used. For small Re and St, up to 30 000 time-steps per period were used; fewer time-steps are needed for larger Re and St.

B. Analytic interfacial solution for $Bo \to \infty$

In the limit $Bo \to \infty$, the interfacial hydrodynamics decouples from the bulk hydrodynamics (but the bulk remains coupled to the interface), and (9) reduces to

$$\frac{\partial^2 v}{\partial r^2} + \frac{1}{r}\frac{\partial v}{\partial r} - \frac{v}{r^2} = 0, \tag{11}$$

which has a simple analytic solution of the form $v = Ar + B/r$, where A and B depend only on the geometric parameters A_R and ϵ and the boundary conditions. When the boundary conditions are time-dependent, so are A and B. In the region inside the knife edge, $r \in [0, 1-\epsilon)$, the solution is $v(r,t) = r\sin(St\,t)$ so that the interface on the inside acts exactly the same as an oscillating disk. Hence, in the limit $Bo \to \infty$, ϵ is irrelevant, and the knife edge together with the highly viscous monolayer are equivalent to a solid disk. In the region outside the knife edge, $r \in (1, A_R)$, the interfacial velocity is

$$v(r,t) = \frac{(r^2 - A_R^2)}{r(1-A_R^2)}\sin(St\,t), \tag{12}$$

so that the interfacial flow is exactly in phase with the forcing of the oscillatory knife edge, and hence the flow at the interface has no phase lag in this limit. The bulk flow that is driven by the oscillatory knife edge and the viscous monolayer do not need to be in phase with the knife edge oscillations, and in fact will not be except in the inertialess limit $Re \to 0$. For finite Bo the interface is not in phase with the knife edge since it is also coupled to the bulk flow, and then to determine the interfacial flow the fully coupled nonlinear system needs to be solved.

C. Symmetries of the system

The system, comprised of the Navier–Stokes equation (3), (4) and (5) together with the boundary conditions (8), (9) and (10), has a half-period-flip spatio-temporal symmetry $\mathcal{H}$.

The action of $\mathcal{H}$ on the velocity is

$$\mathcal{H}(u, v, w)(r, z, t) = (u, -v, w)(r, z, t + T/2), \tag{13}$$

where $T = 2\pi/St$ is the dimensionless oscillation period. The solutions are invariant to this symmetry for all Re, St and Bo considered. For zero phase lag, the velocity would need to satisfy

$$(u, v, w)(r, z, t) = (u, v, w)(r, z, T/2 - t). \tag{14}$$

This is not satisfied for any finite Bo, it is only satisfied in the limit $Bo \to \infty$.

III. EXPERIMENTAL APPARATUS AND METHODS

The present knife-edge viscometer flow apparatus is similar to the device described in detail elsewhere [25], and only the salient features and differences are presented here. The cylinder was made from precision-bore glass of diameter $2aA_R = 50.0\,\mathrm{mm}$ and height $aA_H = 25.4\,\mathrm{mm}$. The glass cylinder was bonded to a floor made of optical glass. The knife edge was made from precision stainless steel bushing stock with outer diameter $2a = 9.53\,\mathrm{mm}$ and thickness ratio $\epsilon = 0.167$. Harmonic oscillations of the knife edge were achieved through a two-step process. First, steady rotational motion of a flywheel driven by a micro-stepper motor was converted to linear harmonic motion using a crankshaft-connecting rod assembly, as described in [26]. The linear harmonic motion was then converted to rotational harmonic motion by a wheel and rail assembly. Harmonic rotation of the knife edge was verified using a rotary encoder and high speed camera, and was found to be within 98% of a pure sine wave. For experiments with steady motion, the knife edge was driven directly by a micro-stepper motor, through a set of pulleys and a timing belt.

The experiments were performed using de-ionized (DI) water at $22.5 \pm 0.5°\mathrm{C}$, with $\nu = 9.46 \times 10^{-3}\,\mathrm{cm}^2/\mathrm{s}$, and $\mu = 9.44 \times 10^{-3}\,\mathrm{g}/(\mathrm{cm\,s})$. The glass dish was cleaned with reagent-grade acetone, then with HPLC-grade methanol, and finally with DI water before each experiment. Stearic acid (Sigma Aldrich, S4751-1G) was dissolved in HPLC-grade benzene and spread on the surface of the water via a gas-tight, glass micro-syringe. Benzene, which is essentially insoluble in water, evaporates quickly, leaving behind a monolayer of stearic acid which was allowed to equilibrate for 15 minutes. The knife edge was then gradually lowered

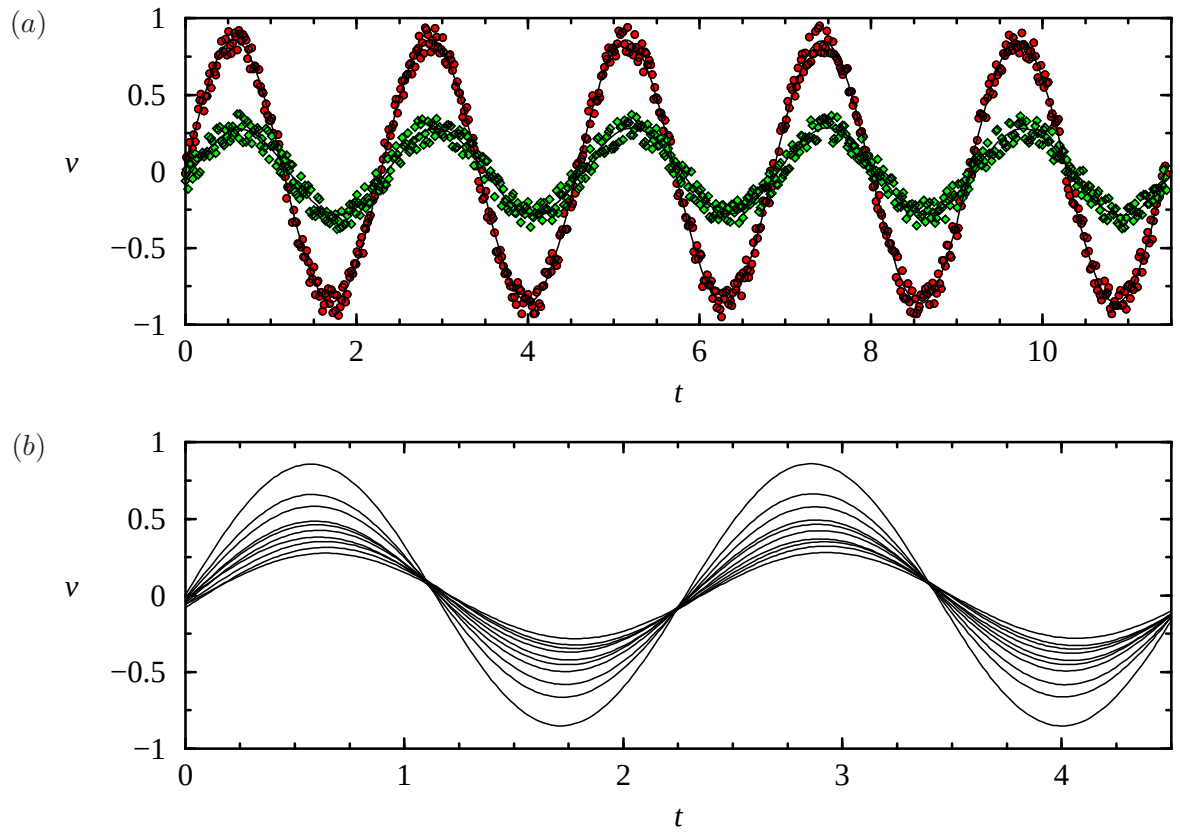

FIG. 2. Time-series of (a) interfacial azimuthal velocity measured at $r = 1.01$ (red circles) and $r = 1.19$ (green diamonds), together with sinusoid fits, and (b) fits to measured data at $r = 1.01 + 0.02j$, $j \in [0, 9]$, all for a stearic acid monolayer of $c = 1$ mg/m^2 driven at $Re = 16$ and $St = 2.5$.

to make contact with the monolayer-covered interface but not penetrate into the bulk. The technique for spreading monolayers of stearic acid on water was independently validated through measurements of the equation of state (the relationship between the surface tension and surface packing of the monolayer) through slow compression in a Langmuir trough. The measurements showed that stearic acid remains a monolayer for concentrations considered here, $c \leq 2\,\mathrm{mg/m^2}$, and it collapses for $c \gtrsim 2.3\,\mathrm{mg/m^2}$ (i.e. $20\,\mathrm{\AA}^2$ per molecule), in agreement with the findings in [27, 28].

The interfacial flow field was measured via particle tracking velocimetry. In order to minimize the effects of seeding particles on the interface, $3\,\mu$m diameter non-wetting particles made out of PTFE (Polysciences Inc., Microdispers–3000) were sparsely distributed on the surface. Prior to their use, the seeding particles were washed twice with reagent-grade acetone in a clean glass petri dish. The supernatant acetone was aspirated, leaving the

particles at the bottom, which were then air dried. After spreading the stearic acid monolayer at the air-water interface and allowing it to equilibrate, the dried PTFE particles were shaken off a clean, dry spatula onto the interface. The coverage of particles was approximately 0.1% of the total surface area. Direct imaging of the PTFE particle motion was performed using a microscope zoom lens (Thales–Optem, 70XL) with a right-angle prism. The images were captured by a black-and-white video camera (Basler, acA2000–165 μm) at frame rates between 40 and 100 fps. For the oscillatory flow measurements, particle motion was recorded over five periods of oscillations. These measurements were made at least 10 minutes (600 s) after the knife edge was set in motion. The time between starting the flow and taking measurements is much larger than the viscous time based on the radius of the knife edge ($a^2/\nu = 24\,\mathrm{s}$) and is comparable to the viscous time based on the full extent of the dish ($a^2 A_R^2/\nu = a^2 A_H^2/\nu = 660\,\mathrm{s}$). For the steady flow measurements, images were captured for 20 s.

For the oscillatory flow measurements, which were performed near the knife edge ($1 < r < 1.2$), the sequence of high-magnification images were processed using ImageJ and Python and tracked using Dlib C$_{++}$ library. MATLAB was used to obtain phase-averaged measurements of the interfacial velocity at various locations near the knife edge to determine the phase shift of the harmonic motion relative to the harmonic motion of the knife edge itself. For measurements when the knife edge was driven steady, a smaller magnification was used to enable visualization of the surface over a region ten times as wide, namely $1 < r < 3$.

Table I presents the parameters used to control the oscillations of the knife edge in the experiments in order to achieve various combinations of (Re, St), all with the fixed values of a, A_R and A_H. The parameters were selected in order to obtain at least an order of magnitude variation in both Re and St. An example of the oscillatory flow measurements is presented in Fig. 2 for a representative value of Re and St. Figure 2(a) shows the nondimensional instantaneous azimuthal velocity as a function of time for two points, one very near the knife edge at $r = 1.01$ and the other at $r = 1.19$. There is a fair amount of noise in the measurements of the velocity, especially at the larger radius. A sinusoid fit to each set of measurements is also presented in the figure. Sinusoidal fits to azimuthal velocity measurements taken in between these locations ($1.01 \leq r \leq 1.19$) are presented in Fig. 2(b). The fits have a correlation coefficient of better than 0.98. The decrease in amplitude with increasing radial distance from the knife edge is as expected. The key point however is the

Re	St	period	sweep
4	2.5	14 s	21°
16	2.5	3.6 s	21°
32	2.5	1.8 s	21°
48	2.5	1.2 s	21°
16	0.5	18 s	110°
16	1.2	7.8 s	48°
16	5.5	1.7 s	10°

TABLE I. Parameters of the oscillatory flow experiments, Reynolds number Re and Stokes number St, together with the corresponding dimensional period of oscillation and sweep angle of the knife edge.

fact that the maxima occur at slightly increasing times with distance from the knife edge. This shows that the interfacial velocity response has a phase lag with respect to the knife edge oscillation, ϕ [degrees], where the phase lag is determined relative to a sinusoid fit to the velocity of the knife edge itself, which is measured simultaneously with the interfacial velocity.

IV. RESULTS

A. Numerical

The results presented in this subsection provide an overview of the flow; additional numerical results corresponding to the experimental cases investigated are presented in tandem with the experimental measurements in the following subsection. We begin here by considering how the system behaves for a range of Re, St and Bo. For sufficiently small Re and St, inertial effects are expected to be small, and for sufficiently large Bo, the interfacial flow is expected to be independent of the bulk flow.

Figure 3 shows the instantaneous azimuthal surface velocity profiles computed at various times over one period for $Re = 4$ and $St = 2.5$ for three values of Bo; this is the lowest Re considered in the experiments. Profiles in red correspond to times when the knife edge is

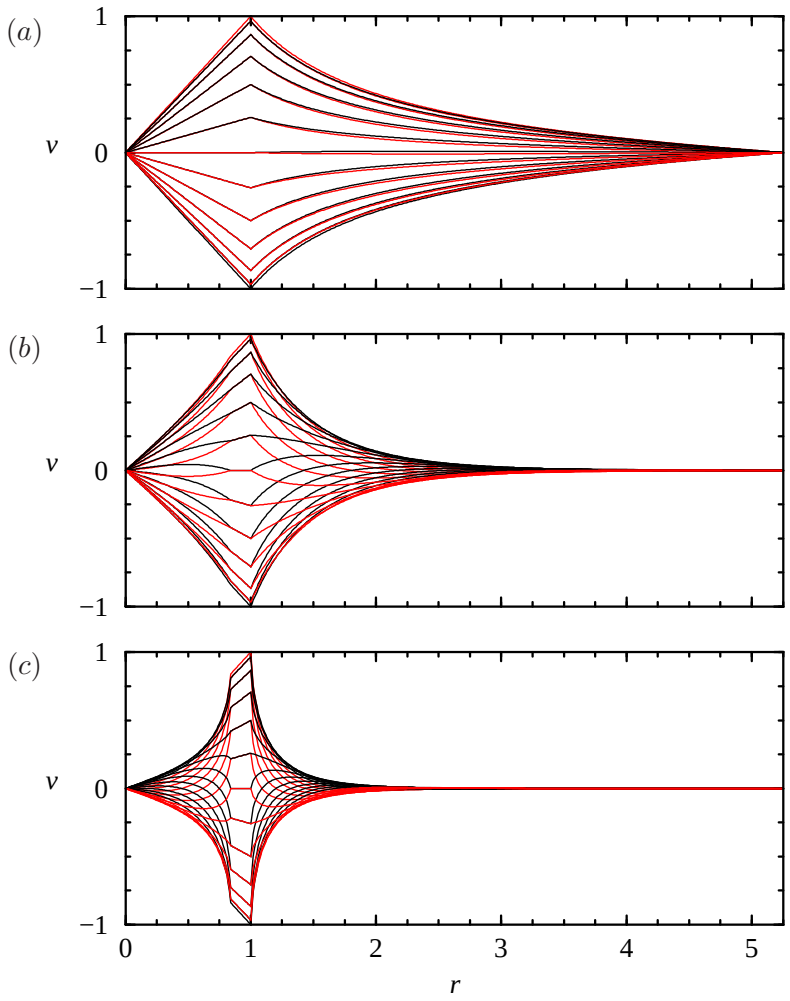

FIG. 3. Computed profiles of azimuthal surface velocity over one period for (a) $Bo = 100$, (b) $Bo = 1$, and (c) $Bo = 0.01$, all with $Re = 4$, $St = 2.5$.

rotating in one direction and those in black are for the return stroke. For a highly viscous interface, with $Bo = 100$, Fig. 3(a) shows that the interface moves essentially in unison with the knife edge. There is very little phase lag visible in the region inside the knife edge and only a slight phase lag is barely detectable in the outside region, as the forward and return stroke profiles do not coincide exactly. The large surface shear viscosity in this case essentially decouples the motion at the interface from the bulk and the interfacial flow extends all the way to the cylinder wall. The interfacial velocity profiles $v(r, t)$ are very close to the analytical profiles described in § II B. This indicates that for this system, $Bo = 100$ is close to the $Bo \to \infty$ limit. For a modest value of surface shear viscosity ($Bo = 1$), Fig. 3(b) shows significant coupling between the interfacial and bulk flows, even at such a

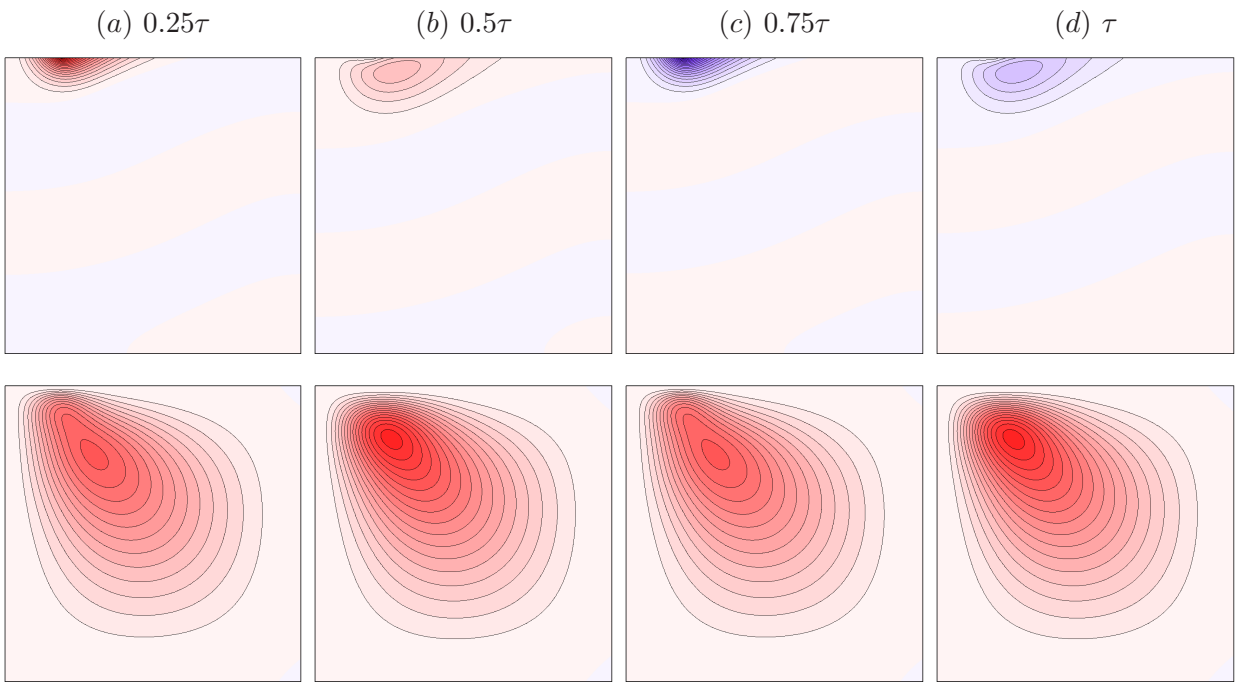

FIG. 4. Snapshots of vortex lines (contours of rv; top row) and streamlines (contours of ψ; bottom row) over one period for $Re = 4$, $St = 2.5$ and $Bo = 1$. There are 20 positive (red) and 20 negative (blue) contour levels in the range $rv \in [-0.2, 0.2]$ and $\psi \in [-0.006, 0.006]$. See supplemental Material at [URL will be inserted by publisher] for animations.

small Reynolds number ($Re = 4$). There is significant phase lag both in the regions inside and outside the knife edge. Unlike the high surface shear viscosity case, the interface in the region inside the knife edge is not in solid-body rotation and the motion outside the knife edge dies out by $r \approx 3.5$, about half way between the oscillating knife and the stationary cylinder wall. Figure 3(c) shows that when the interface has very low viscosity ($Bo = 0.01$), the interfacial velocity is dominated by the finite inertia of the bulk liquid, exhibiting large phase lag and highly nonlinear velocity profiles in the region inside the knife edge and that the flow diminishes rapidly away from the knife edge, with $v(r, t) \to 0$ for $r \gtrsim 2$.

Snapshots of the flow in the bulk corresponding to the $Bo = 1$ case are presented in Fig. 4 for four instants over one period (see Supplemental Material at [URL will be inserted by publisher] for animations). The top row shows the vortex lines (contours of angular momentum rv) and the bottom row shows the streamlines. Panel (a) in the figure shows the flow at the instant when the knife edge is at its maximum speed going in one direction

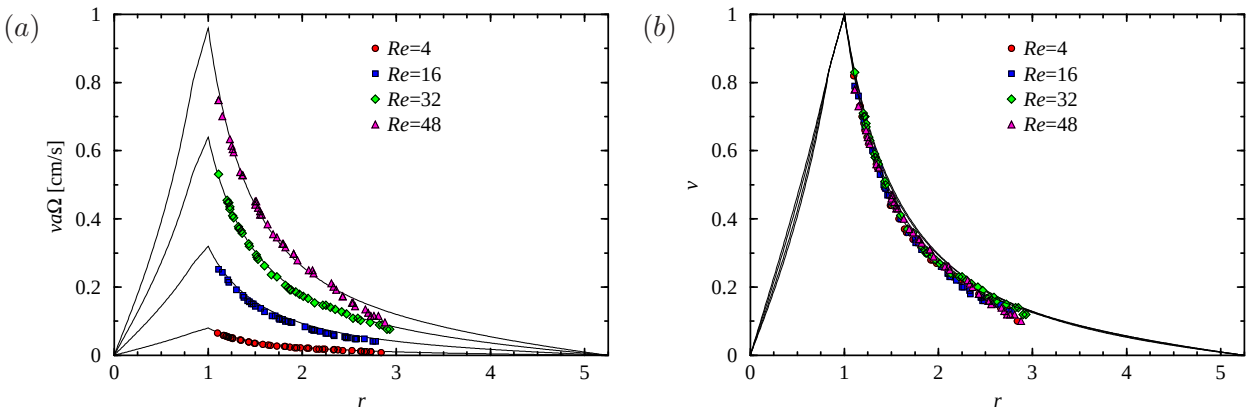

FIG. 5. Azimuthal velocity profiles at the interface with a stearic acid monolayer at surface concentration $c = 1\,\mathrm{mg/m^2}$ for Re as indicated. The symbols are experimental measurements and the curves are computed with $Bo = 1$ and the corresponding Re; (a) presents the data in dimensional form and in (b) the data has been nondimensionalized.

and panel (c) shows the flow when the knife edge is at its maximum speed in the return stroke. Panels (b) and (d) show the bulk flow at the instant when the knife edge is stopped, exhibiting the diffusion of the vortex lines into the bulk. The finite angle at which the vortex lines meet the surface is consistent with an interface with a finite surface shear viscosity [19]. The streamlines in the figure exhibit the well-known large-scale meridional mean streaming flow that is expected for a torsionally oscillating disk, independent of the viscosity [29–32]. Interestingly, the figure shows that the streaming is at its strongest at the end of the stroke, when the knife edge is stopped and is about to reverse its direction of rotation (panels b and d). The flow is invariant to the half-period-flip symmetry $\mathcal{H}$ (13).

B. Experimental

1. *Steady-driven flow*

We begin by detailing the measurements of the steady-driven knife edge ($St = 0$) since these have received much attention recently and can serve as a baseline [17, 25]. Figure 5(a) shows the measured azimuthal velocity profiles for a monolayer of stearic acid at surface concentration $c = 1\,\mathrm{mg/m^2}$ for $4 \leq Re \leq 48$. For each Reynolds number, numerical predictions with a single value of $Bo = 1$ are also presented in the figure; part (b) of the figure

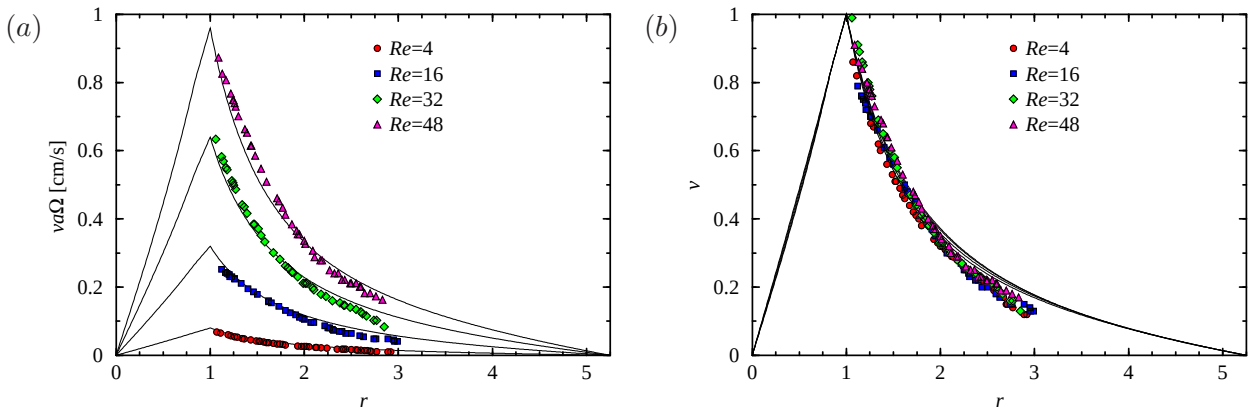

FIG. 6. Azimuthal velocity profiles at the interface with a stearic acid monolayer at surface concentration $c = 2\,\mathrm{mg/m^2}$ for Re as indicated. The symbols are experimental measurements and the curves are computed with $Bo = 3.0$ and the corresponding Re; (a) presents the data in dimensional form and in (b) the data has been nondimensionalized.

presents these velocity measurements in dimensionless form. Note that the flow shows a small dependence on Re due to the modest value of Bo coupling the interfacial and bulk flows. The good agreement between the measurements and computations at $Bo = 1$ indicate that the dimensional surface shear viscosity is $\mu^s = 0.003\,\mathrm{g/s}$ (surface Poise), which falls in the range reported in the literature for stearic acid at $c = 1\,\mathrm{mg/m^2}$ [21, 27, 33]. Finally, it should be noted that interfacial velocity measurements show that the radial component is zero, to within experimental uncertainty. This is consistent with prior experiments [25], and validates the zero radial flow assumption used in the present model.

Measurements of the interfacial velocity for the stearic acid monolayers at surface concentration $c = 2\,\mathrm{mg/m^2}$ exhibit a much more viscous response, as expected. Figure 6 shows that the measurements compare reasonably well to computations using $Bo = 3.0$. The nondimensionalized velocity profiles show very little Reynolds number dependence, as expected for a more viscous interface [17]. The computations also illustrate that the flow inside the knife edge is indistinguishable from solid body rotation. Unlike the lower concentration monolayer case, now with $c = 2\,\mathrm{mg/m^2}$ there is a slight difference in the measured shape of the velocity profiles and the computed profiles at large radii. Near the knife edge, $1 < r \lesssim 2$, simulations with $Bo = 3.0$ fit the velocity measurements very well, but progressively with increased distance from the knife edge, the velocity measurements are smaller than those predicted by

the Newtonian interfacial model, see Fig. 6(b). The shape of the measured velocity profile is consistent with an interface exhibiting some degree of shear-thinning; the monolayer tends to flow readily near the knife edge where the shear rate is large, but tends to freeze near the stationary cylinder wall where the shear rate is small. The departure from a Newtonian response observed in this case ($c = 2\,\mathrm{mg/m^2}$) is not surprising given the close proximity to the surface concentration where the monolayer transitions to a solid phase before collapsing at surface concentration $c \approx 2.3\,\mathrm{mg/m^2}$ [27].

2. Oscillatory-driven flow

Figure 7 shows comparisons between measured and computed phases just outside the knife edge, where high resolution, time-resolved measurements of the azimuthal velocity were made. Measurements with stearic acid monolayers at two concentrations ($c = 1$ and $c = 2\,\mathrm{mg/m^2}$) are presented for the Re and St values listed in Table I. As expected, the phase lag is consistently smaller for a monolayer with larger surface packing, indicative of a larger surface shear viscosity. The measurements of the phase lag for stearic acid at $c = 1\,\mathrm{mg/m^2}$ correlate well to computations with $Bo = 1$ for all combinations of (Re, St), and measurements at concentration $c = 2\,\mathrm{mg/m^2}$ correlate to $Bo = 3$. This is in agreement with the steady experimental results.

The salient feature of Fig. 7 is that in every case, the phase lag varies linearly with radial distance from the knife edge. Figure 7 also shows that the phase lag steepens with increasing Re and with increasing St. The phase lag decreases with increasing Bo since a more viscous interface reduces the influence of the bulk flow on the interfacial hydrodynamics. This is to be expected since in the limit $Bo \to \infty$ the phase lag is zero throughout the interface.

Since the phase lag increases linearly with r near the knife edge, there is a well-defined $\phi_r = \partial\phi/\partial r$ that is a function Re, St and Bo. The computed ϕ_r is presented in Fig. 8, which shows that ϕ_r scales with $Bo^{-1/2}$, both when St is kept fixed (panel a) and when Re is kept fixed (panel b). The $-1/2$ power scaling is not surprising since $Bo = \mu^s/\mu a$ is proportional to the surface shear viscosity (both the length scale and the viscosity in the bulk are constant in the current experiments), and scaling with viscosity to the $-1/2$ power is typical [34]. In particular, ϕ_r near the knife edge may be interpreted by analogy with the similarity solution for a wall oscillating harmonically in its own plane, the so-called Stokes' second problem.

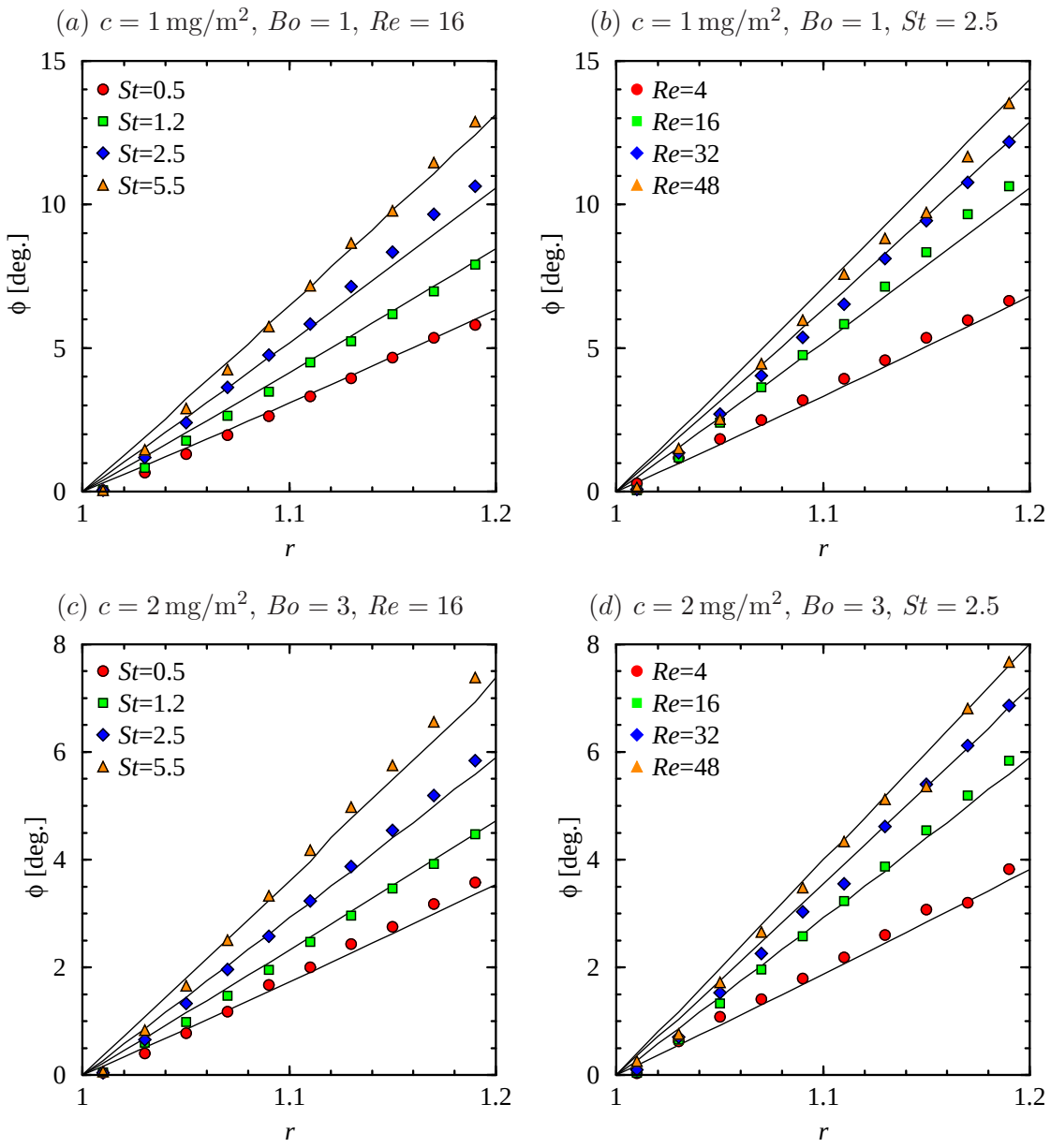

FIG. 7. Radial distribution of the phase lag between the interfacial azimuthal velocity and the knife edge, for Re and St as indicated. Experimental measurements are for stearic acid monolayers at surface concentrations c as indicated (symbols), and the solid curves are the corresponding computations at Bo as indicated.

That solution shows that the phase lag is linearly proportional to the distance from the oscillating wall and proportional to viscosity to the $-1/2$ power.

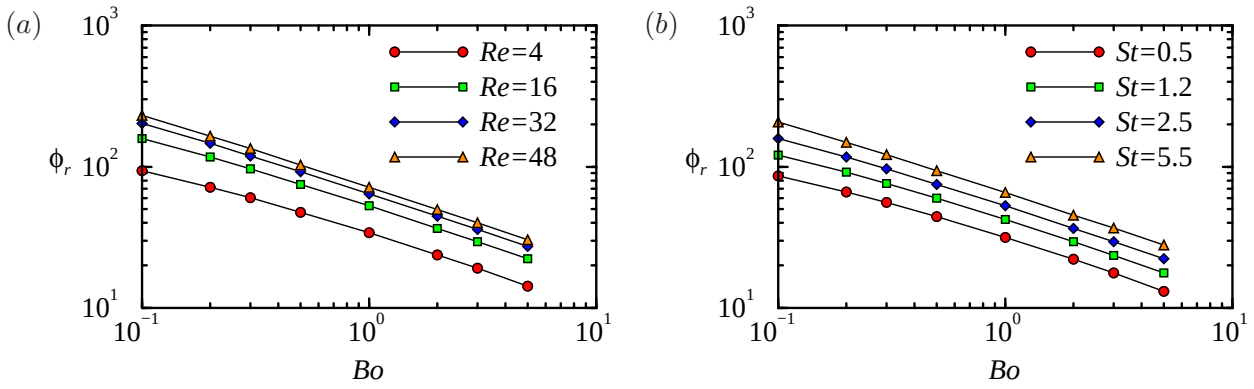

FIG. 8. Computed values of the radial gradient of the phase lag, ϕ_r, versus Bo for (a) $St = 2.5$ and Re as indicated, and (b) $Re = 16$ and St as indicated. The symbols represent numerical cases computed.

V. CONCLUSIONS

The classic Boussinesq–Scriven surface model has been coupled to the Navier–Stokes equations for flow in a cylindrical geometry, fully accounting for the secondary flow resulting from the curved geometry, and a numerical solution procedure has been developed to predict the flow when the interface is subjected to unsteady shear. The numerical results have been verified and validated against experiments using a widely studied monolayer, stearic acid, that is known to have a viscous Newtonian response to steady shear. The experiments, and the corresponding numerical simulations, were conducted using the knife edge viscometer flow geometry. We have predicted and verified the response to oscillatory forcing, considering an order of magnitude range in the forcing amplitude and frequency, and show that for a given surface concentration of the monolayer, a single value of surface shear viscosity collapses the oscillatory cases independent of amplitude and frequency of the forcing, and that the value of the surface shear viscosity agrees with value that is found under steady shearing.

The flow at the interface is uni-directional, i.e. in the azimuthal direction, but the flow in the bulk has a significant secondary meridional overturning component. The oscillatory forcing at the interface drives a steady streaming flow in the bulk. If the surface shear viscosity of the monolayer is extremely large, the interfacial flow is oblivious to the bulk flow. However, for finite surface shear viscosities, the interfacial and bulk flows are viscously

coupled, and the details of the bulk flow need to be accounted for in order to predict the interfacial flow correctly.

The interfacial velocity in the vicinity of the knife edge was found to have a phase lag that varied linearly with radial distance from the knife edge. The phase lag becomes steeper with both increasing forcing amplitude and frequency. The slope of the phase lag was found to scale with the surface shear viscosity to the $-1/2$ power, which is analagous to the classic solution for a wall harmonically oscillating in its own plane. The variation of the radial gradient of the phase lag with surface shear viscosity μ^s is much greater than the variation with μ^s of the interfacial velocity profile under steady shearing, indicating that the knife edge viscometer is more sensitive when harmonically forced.

ACKNOWLEDGMENTS

We thank William F. Flaherty for machining the parts of the flow apparatus and Joseph A. Adam for his contributions to the experiments. This work was supported by NASA grant NNX13AQ22G.

[1] R. H. Notter, *Lung Surfactants: Basic Science and Clinical Applications*, volume 149 of *Lung Biology in Health and Disease*. Marcel Dekker (2000).

[2] E. J. A. Veldhuizen and H. P. Haagsman, *Review: Role of pulmonary surfactant components in surface film formation and dynamics*. Biochimica et Biophysica Acta **1467**, 255 (2000).

[3] J. A. Zasadzinski, J. Ding, H. E. Warriner, F. Bringezu, and A. J. Waring, *The physics and physiology of lung surfactants*. Current Opinion in Colloid & Interfacial Sci. **6**, 506 (2001).

[4] E. Hermans, M. S. Bhamla, P. Kao, G. G. Fuller, and J. Vermant, *Lung surfactants and different contributions to thin film stability*. Soft Matter **11**, 8048 (2015).

[5] N. M. Frew. The role of organic films in air-sea gas exchange. in P. S. Liss and R. A. Duce, editors, *The Sea Surface and Global Change*, chapter 5, p. 121. Cambridge Univ. Press, (1997).

[6] W.-T. Tsai and K.-K. Liu, *An assessment of the effect of sea surface surfactant on global atmosphere-ocean CO_2 flux*. J. Geophys. Res. **108**, C4, 3127 (2003).

[7] R. J. Lee and J. R. Saylor, *The effect of a surfactant monolayer on oxygen transfer across an*

air/water interface during mixed convection. Intnl J. Heat Mass Transfer **53**, 3405 (2010).

[8] M. E. Salter, R. C. Upstill-Goddard, P. D. Nightingale, S. D. Archer, B. Blomquist, D. T. Ho, B. Huebert, P. Schlosser, and M. Yang, *Impact of an artificial surfactant release on air-sea gas fluxes during Deep Ocean Gas Exchange Experiment II.* J. Geophys. Res. **116**, C11016 (2011).

[9] X. D. Zhang, C. W. Macosko, H. T. Davis, A. D. Nikolov, and D. T. Wasan, *Role of silicone surfactant in flexible polyurethane foam.* J. Colloid Interface Sci. **215**, 270 (1999).

[10] S. A. Snow, U. C. Pernisz, and R. J. Braun, *"Tying up loose ends" – silicone surfactants as stabilizing agents for flexible polyurethane foam.* Silicon Chem. **3**, 1 (2005).

[11] B. Zhmud and F. Tiberg. Surfactants in ink-jet inks. in D. R. Karsa, editor, *Surfactants in Polymers, Coatings, Inks and Adhesives*, chapter 8, p. 1. Blackwell Publishing, England, (2003).

[12] Y.-C. Liao, H. J. Subramani, E. I. Franses, and O. A. Basaran, *Effects of soluble surfactants on the deformation and breakup of stretching liquid bridges.* Langmuir **20**, 9926 (2004).

[13] T. F. Tadros. Surfactants in the food industry. in *Applied Surfactants: Principles and Applications*, chapter 15. Wiley, (2005).

[14] I. Kralova and J. Sjöblom, *Surfactants used in food industry: a review.* J. Dispersion Sci. Tech. **30** (2009).

[15] D. G. Hayes. Bioprocessing methods to prepare biobased surfactants for pharmaceutical products. American Pharmaceutical Rev., (2011). http://www.-americanpharmaceuticalreview.com/Featured-Articles/37032-Bioprocessing-Methods-to-Prepare-Biobased-Surfactants-for-Pharmaceutical-Products/.

[16] T. Verwijlen, P. Moldenaers, H. A. Stone, and J. Vermant, *Study of the flow field in the magnetic rod interfacial stress rheometer.* Langmuir **27**, 9345 (2011).

[17] J. M. Lopez and A. H. Hirsa, *Coupling of the interfacial and bulk flow in knife-edge viscometers.* Phys. Fluids **27**, 042102 (2015).

[18] S. Vandebril, A. Franck, G. G. Fuller, P. Moldnaers, and J. Vermant, *A double wall-ring geometry for interfacial shear rheology.* Rheol. Acta **49**, 131 (2010).

[19] A. H. Hirsa, J. M. Lopez, and R. Miraghaie, *Determination of surface shear viscosity via deep-channel flow with inertia.* J. Fluid Mech. **470**, 135 (2002).

[20] L. E. Scriven, *Dynamics of a fluid interface.* Chem. Engng. Sci. **12**, 98 (1960).

[21] D. A. Edwards, H. Brenner, and D. T. Wasan, *Interfacial Transport Processes and Rheology*. Butterworth-Heinemann, Boston (1991).

[22] J. C. Slattery, L. Sagis, and E.-S. Oh, *Interfacial Transport Phenomena*. Springer: New York, second edition (2007).

[23] J. M. Lopez, *Axisymmetric vortex breakdown: Part 1. Confined swirling flow*. J. Fluid Mech. **221**, 533 (1990).

[24] J. M. Lopez and A. Hirsa, *Surfactant influenced gas/liquid interfaces: Nonlinear equation of state and finite surface viscosities*. J. Colloid Interface Sci. **229**, 575 (2000).

[25] A. Raghunandan, J. M. Lopez, and A. H. Hirsa, *Bulk flow driven by a viscous monolayer*. J. Fluid Mech. **785**, 283 (2015).

[26] J. J. F. Leung, A. H. Hirsa, H. M. Blackburn, F. Marques, and J. M. Lopez, *Three-dimensional modes in a periodically driven elongated cavity*. Phys. Rev. E **71**, 026305 (2005).

[27] A. Poskanzer and F. C. Goodrich, *A new surface viscometer of high sensitivity: II. Experiments with stearic acid monolayers*. J. Colloid Interface Sci. **52**, 213 (1975).

[28] M. J. Vogel and A. H. Hirsa, *Concentration measurements downstream of an insoluble monolayer front*. J. Fluid Mech. **472**, 283 (2002).

[29] S. Rosenblat, *Torsional oscillations of a plane in a viscous fluid*. J. Fluid Mech. **6**, 206 (1959).

[30] D. J. Benney, *The flow induced by a disk oscillating in its own plane*. J. Fluid Mech. **18**, 385 (1964).

[31] C.-S. Yih, *Fluid Mechanics*. West River Press: Ann Arbour, Michigan (1977).

[32] A. Rubio, J. M. Lopez, and F. Marques, *Interacting oscillatory boundary layers and wall modes in modulated rotating convection*. J. Fluid Mech. **625**, 75 (2009).

[33] H. C. Maru and D. T. Wasan, *Dilational viscoelastic properties of fluid interfaces-II*. Chemical Engr. Sci. **34**, 1295 (1979).

[34] H. Schlichting and K. Gersten, *Boundary-Layer Theory*. Springer, eighth edition (2003).